Integrated use of GPS and EGNOS Carrier Phase Observations for High Precision Kinematic Positioning[1]

K Sauer and W Y Ochieng
Imperial College, London, United Kingdom

Abstract

Real-time satellite positioning at the sub-decimeter or even sub-centimeter level of accuracy requires the use of carrier phase data. However, in harsh operational environments such as those encountered in engineering environments, often the number and geometry of available satellites are insufficient, due to signal blockage. Combined use of GPS dual frequency and EGNOS single frequency carrier phase data should provide a degree of increased reliability and availability of positioning with carrier phase. To exploit this to a full extent, the different error sources should be reduced significantly. This paper assesses the possibility of creating a local ionospheric model for the EGNOS single frequency data, using GPS dual frequency measurements, a Kalman filter and a weighted 2-D biharmonic spline interpolation algorithm. The results show that the local ionospheric model can facilitate significantly, the correct determination of integer ambiguities particularly in those cases where some GPS satellites are unavailable due to blockage.

1 INTRODUCTION

The reliability and availability of carrier phase ambiguity determination is dependent on the availability and geometry of satellites, and the errors inherent in the measurements. In harsh operational situations such as those encountered in engineering environments, often the number and geometry of available satellites are insufficient, due to signal blockage.

Combined use of GPS dual frequency and EGNOS single frequency carrier phase data should provide a degree of increased reliability and availability of positioning with carrier phase. To exploit this to a full extent, the different error sources should be modelled and reduced significantly. The fact that EGNOS satellites broadcast only on a single frequency (the same as GPS L1) imposes the need to determine a model to generate the corrections for the impact of the ionosphere on the measurements. This is true particularly in periods of extended geomagnetic activity and when baseline lengths exceed a few tens of kilometres (Hansen et al., 2000).

Existing strategies that could be applicable to the GEO single frequency ionospheric problem range from the application of the Klobuchar model (transmitted in the navigation message) to local or regional models generated from dual frequency GPS data from several reference stations. For example, Hernandes-Pajares et al. (2000) have implemented an ionospheric tomography algorithm to provide ionospheric corrections for single frequency users. However, under certain practical circumstances there may neither be a sufficient number of reference stations available for the determination of such regional models nor real-time data transmission capacity for ionospheric corrections to enable real-time positioning with carrier phase data. Furthermore, the properties of existing standard and regional ionospheric models may be insufficient for carrier phase applications. In general such models are based on post-processing algorithms which include rather large areas (global and regional models) with a spatial resolution of >2.5 degree (≈ 280km) and a temporal resolution of ~ 1h. They are available with a considerable temporal delay of >24h (Feltens et. al. 1998). In such cases, a local ionospheric model based on a 2-dimensional biharmonic spline interpolation could provide an optimal prediction using sparsely spaced dual-frequency GPS derived ionospheric delay data points (Sandwell, 1987).

---

[1] This paper has been presented at the GNSS 2002 conference in Copenhagen; Denmark, 27.-30. May 2002

The biharmonic spline approach enables any noisy dual frequency based ionospheric delay data to be de-weighted accordingly enabling all data to contribute according to its quality while maintaining a strong geometric configuration. This is realised by evaluating a Green's force function using a weight assigned particularly to each data point (Sandwell, 1987).

The research highlighted here has studied the possibility of creating a local ionospheric model for the EGNOS single frequency data, using GPS dual frequency measurements, a Kalman filter and a weighted 2-D biharmonic spline interpolation algorithm.

The process adopted is shown in Figure 1 and involves the determination of ionospheric delays from dual frequency GPS data at various ionospheric pierce points (IPP) for a given pair of stations at an instant in time (after the Kalman filter has converged) using a Kalman filter and then modelling spatially using a 2-D biharmonic spline interpolation technique. The resulting model is then used to determine the ionospheric delay for the GEO L1 data. This is followed by the determination of the unknowns including antenna position and integer ambiguities. The approach developed uses least-square filtering to capture the temporal ionospheric behaviour based on the idea by Goad (1990). The idea describes the use of L1/L2 P-code and carrier-phase observations to predict the slant ionospheric delay using a weighted Bayesian filter algorithm. Based on this approach the presented research develops a weighted Kalman-filter to evaluate the ionospheric delays and to reduce the level of noise that could propagate into the determination of the delays at the various IPPs. The modelling strategy (Figure 1) has been tested extensively using synthetic (simulated) dual frequency data. Initial results based on GPS and EGNOS real field data have been produced also. The real field data were captured at 8 stations in the Greater London area using NovAtel Millennium Wide Area Augmentation (WAAS) capable receivers, and processed in a simulated real-time mode (i.e. epoch by epoch).

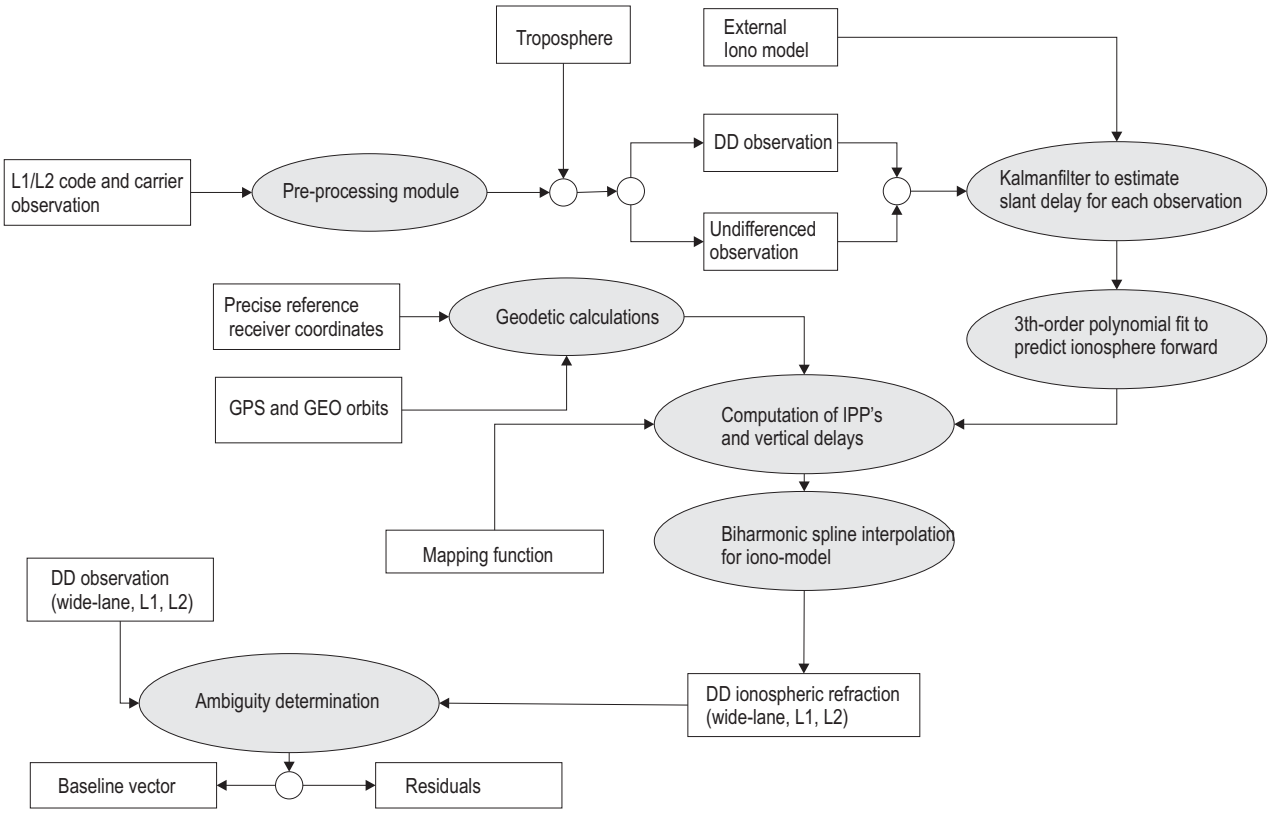

Figure 1: Flowchart for the new processing strategy

Section 2 of the paper looks at the benefit to be gained from the use of EGNOS ranging data with GPS pseudorange data for basic navigation. Section 3 presents the main features of real-time ionospheric filtering using a weighted Kalman filter. Forward prediction and single layer mapping function requirements are covered in Section 4. Parameterisation of the ionospheric delay using biharmonic spline interpolation is discussed in Section 5. The strategy for determining double differenced carrier phase integer ambiguities is presented in Section 6, together with the results using synthetic data. Real field data results are given in Section 7. The paper is concluded in Section 8.

2 ENHANCED NAVIGATION PERFORMANCE USING EGNOS DATA

The European Geostationary Navigation Overlay Service (EGNOS) is being developed to augment GPS. EGNOS comprises of three service levels:

- **GNSS Integrity Channel (GIC):** to improve integrity by the broadcast of satellite/system health status data to users.
- **Wide Area Differential (WAD):** to improve accuracy by the dissemination differential corrections.
- **Geo Ranging (R-GEO):** to improve continuity and availability by the transmission of a GPS like signal from GEO satellites.

The implementation within the EGNOS space segment is realised by two Inmarsat-III satellites (AOR-E and IOR) to cover the European Civil Aviation Conference (ECAC) service region (Loddo et al. 1996) Currently EGNOS is in the testing and validation phase.

Initial studies were carried out to investigate the potential for enhanced navigation performance using the basic observable (i.e. pseudorange) from the EGNOS GEO satellites. A number of scenarios were formulated to capture this including the use of all satellites available above 15^{o} (*scenario 1*), a simulation of a harsh navigation environment where 50% of GPS satellites are *blocked* with the remaining satellites having a degraded geometrical configuration (*scenario 2*), and the same as scenario 2 but with an EGNOS GEO satellite available and visible (*scenario 3*). Table 1 shows the standard deviation of the positional components ($\sigma_{north,95\%}$, $\sigma_{east,95\%}$, $\sigma_{height,95\%}$) for the three scenarios using real GPS and EGNOS GEO data. The statistics have been generated from the differences between the calculated positions and the *true* position determined from GPS carrier phase data processed in static mode.

	Max. HDOP	$\sigma_{north,95\%}$	$\sigma_{east,95\%}$	$\sigma_{heigth,95\%}$
All available Satellites	1.2	1.66	2	3.68
GPS only (50% of all GPS SVs *blocked*)	18.4	7.39	8.28	22.02
GPS (50% blockage) + 1 EGNOS GEO SV	9.4	4.95	4.74	12.47

Table 1: Standard deviations (scaled at 95%) for single point positioning

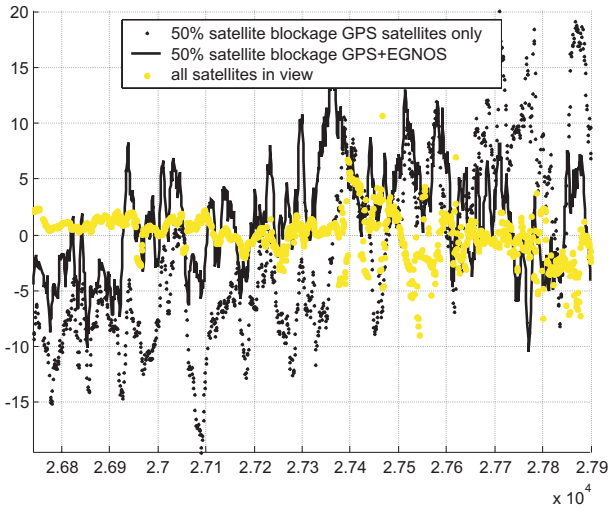

Figure 2: δ_{north} deviation from true position (m)

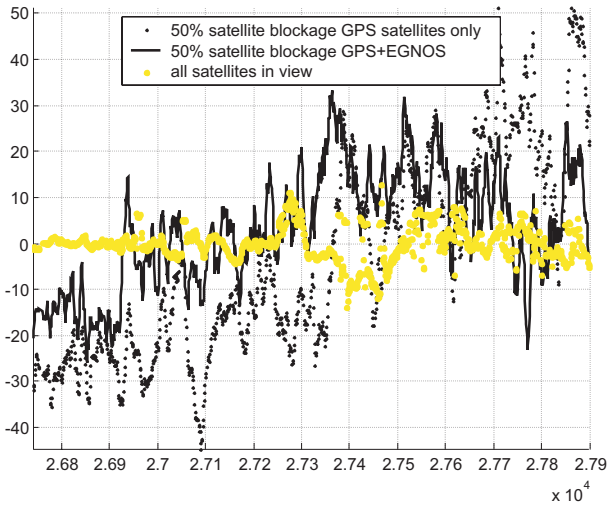

Figure 3: δ_{heigth} deviation from true position (m)

The potential for enhanced navigation performance by the use of EGNOS GEO ranging data can be seen in Table 1 and, Figures 2 and 3. For example, $\sigma_{height,95\%}$ drops from 22.02m in *scenario 2* to 12.5m in *scenario 3*. This level of improvement is significant and justifies further research to investigate the benefit of using EGNOS L1 together with GPS dual frequency carrier-phase data for kinematic positioning.

3 REAL-TIME IONOSPHERIC FILTERING USING A WEIGHTED KALMAN FILTER

Kalman filtering was introduced into GPS processing by Brown and Hwang (1993). Many researchers have subsequently applied it to process GPS data. The idea of using least squares filtering to estimate ionospheric range errors was first published in 1990 (Goad, 1990). Based on this idea and the Kalman filter formulation published by Leick (1995), an algorithm has been developed to predict the short-term temporal behaviour of the ionosphere based on a minimal set of two receivers. Assuming relatively low values of code and carrier noise for both L1 and L2 (Table 2) for the receiver used in the current investigation, it is feasible to combine L1 and L2 code and carrier phase observations between the receiver i and the satellite k as follows (Goad, 1990):

$$
\begin{aligned}
L^k_{i,L1} &= \rho^k_i - (I^k_{i,\varsigma} + I^k_{i,\delta}) + T^k_i + \lambda_{L1} N^k_{i,L1} + \varepsilon^k_{i,\varphi,L1} \\
L^k_{i,L2} &= \rho^k_i - \xi(I^k_{i,\varsigma} + I^k_{i,\delta}) + T^k_i + \lambda_{L2} N^k_{i,L2} + \varepsilon^k_{i,\varphi,L2} \\
PR^k_{i,L1} &= \rho^k_i + (I^k_{i,\varsigma} + I^k_{i,\delta}) + T^k_i + \lambda_{L1} N^k_{i,L1} + \varepsilon^k_{i,PR,L1} \\
PR^k_{i,L1} &= \rho^k_i + \xi(I^k_{i,\varsigma} + I^k_{i,\delta}) + T^k_i + \lambda_{L2} N^k_{i,L2} + \varepsilon^k_{i,PR,L2}
\end{aligned}
\qquad \textit{(1-4)}
$$

The parameter ρ common in all four equations above represents the geometrical distance, N the corresponding integer ambiguity, λ the wavelength and ξ the frequency ratio $f_2^1/f_2^2 \approx 1.647$. The term I_ς represents the stochastic part of the ionosphere and I_δ the deterministic part, which can be interpreted as a trend function.

The application of the above equations to determine the ionospheric delays is based on the tropospheric error, T being reduced by the use of the Saastamoinen model and the clock errors and orbit errors (to a large extent) being accounted for by double differencing. It has been assumed also that the remaining errors summarised as ε (e.g. code and carrier phase multipath) have a *"noise-like"* behaviour. The equations above can be rewritten at all levels of differentiation (i.e the filter runs with either DD-observations or it runs with "one-way" observations whereas the observations are double-differenced at a later stage). The

subdivision of I into a deterministic and a stochastic part enables the optimal use of externally derived ionospheric observations as retrieved from other regional ionospheric models (i.e. WAAS message types 18 and 26, or CODE ionospheric models).

The number filters running continuously is determined by the number of available satellite-receiver combinations. To decrease the time of convergence ionospheric slant delays based on a regional model are introduced as first estimate to initialise the filter. The Kalman state vector contains an estimate for the range, the ionospheric slant delay, the wide-lane ambiguity and an error term.

Frequency	$\sigma_{carrier}$[m]	σ_{code}[m]	C/N_0[dB-Hz]
L1	0.003	0.1	>42.0
L2	0.005	0.4	>36.0

Table 1: Receiver performance parameters for code and carrier measurements for NovAtel GPScard(WAAS) [source: NovAtel Inc. 1997]

4 IONOSPHERIC FORWARD PREDICTION AND SINGLE LAYER MAPPING FUNCTION

4.1 Forward prediction

Based on filtered ionospheric range delays as derived in the previous section it is possible to derive an interpolated ionospheric model directly once the Kalman filter has converged (found in this research to be ~5min for synthetic data and ~20min for real data). A continuously running filter provides current ionospheric range delays feeding into the interpolation module as described in Section 5.

In a practical application scenario (i.e. in building sides with a high level of satellite blockage) the ionospheric filter would not be able to compute ionospheric corrections continuously. To ensure a instantly available corrections and furthermore to ease computational burden the research has assessed a possible forward prediction method using a suitable functional model. For a short time span between model computation and prediction a 6th-order polynom of the form

$$p(x) = p_1 x^n + p_2 x^{n-1} + \ldots + p_n x + p_{n+1} \quad n = 6 \quad (5)$$

has been fitted (in a least-square sense) to the filtered ionospheric range delays. The derived ionospheric function allows the forward prediction of the ionosphere. The time taken by predicted values to drift away significantly depends on the ionospheric/ geomagnetic activity.

4.2 Mapping function

As stated in Section 1 the set of data points is sparsely distributed. Hence a single-layer ionospheric model provides sufficient approximation of the ionosphere. To convert the computed or predicted slant delay $\delta_{ion,slant}$ into vertical delay $\delta_{ion,vert}$ the following mapping function using the shell height H_{shell} and the elevation E has been used.

$$F = \sqrt{1 - \left(\frac{R_{WGS84} \cos E}{R_{WGS84} + H_{shell}} \right)^2} \quad (6)$$

Other single-layer mapping functions are discussed in Schaer (1999). The differences particularly for satellites at high elevations are small and can be neglected.

5 IONOSPHERIC PARAMETRISATION USING BIHARMONIC SPLINE INTERPOLATION

Biharmonic splines are commonly used for the inter-polation/ parametrisation of sparsely distributed data sets. Based on the original idea by Sandwell (1987) a 2-D biharmonic spline interpolation has been realised. For the 2-D case, the following biharmonic spline function returns the interpolated value $\delta_{ion,node}$ (vertical ionospheric delay at the evaluated node-point or the GEO pierce point) using N data-points.

$$\delta_{ion,node} = \sum_{j=1}^{N} \delta_{ion,j} \bullet \phi_m \left(x_{node} - x_j \right)$$

ϕ_m denotes the two-dimensional Green's force function used to evaluate the specific weight of each data point, x_{node} - x_j the vector between the data-point and the evaluated node-point and $\delta_{ion,j}$ the corresponding vertical delay

$$\phi_m = |x| 2 \left(\ln \left| x_{node} - x_j \right| - 1 \right)$$

Although rather sparsely placed data points (10 for a region of 12° ×20°) have been used, the strategy ensures a stable linear system and an optimal estimate (in a least square sense).

Synthetic data has been used to validate the computed ionospheric model. Since the "true" (injected) ionosphere is known it has been compared with the recovered model. As a measure of model recovery the difference between both does not exceed *0.06m* RMS (cf. Figure 4 – Figure 6). However, the rather good model fit is caused by the synthetic data set used which contains only noise like error components. Additionally Figure 4 shows the impact of low satellites (towards the model borders) contributing at a higher level to model uncertainties. The computation of un-differenced ionospheric delay based on real data set leads to a maximum standard deviation of $\sigma_{ion,oneway,95\%} = 0.40m$. The corresponding value for double-differenced ionospheric delay is $\sigma_{ion,dd,95\%} = 0.01m$.

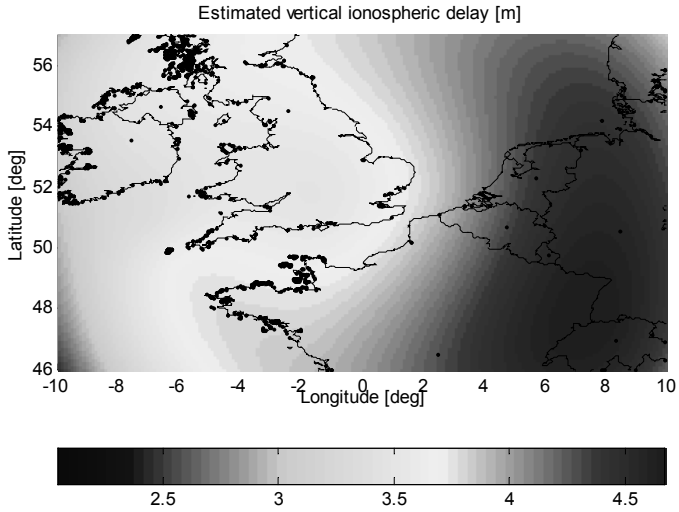

Figure 4: Simulated input vertical ionospheric delays [m]

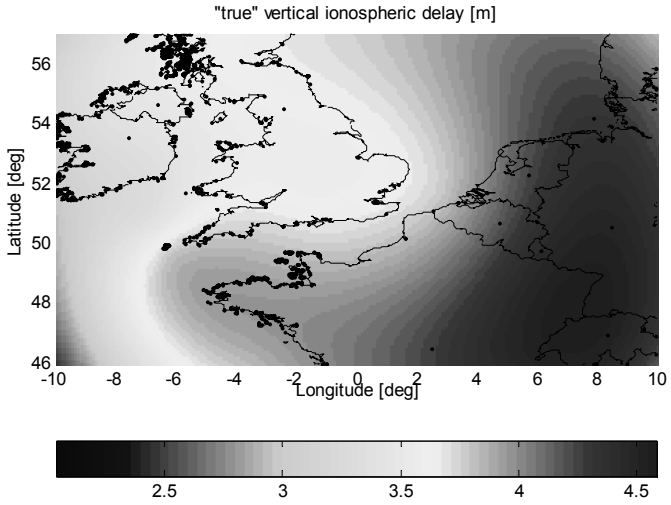

Figure 5: Recovered vertical ionospheric delays[m]

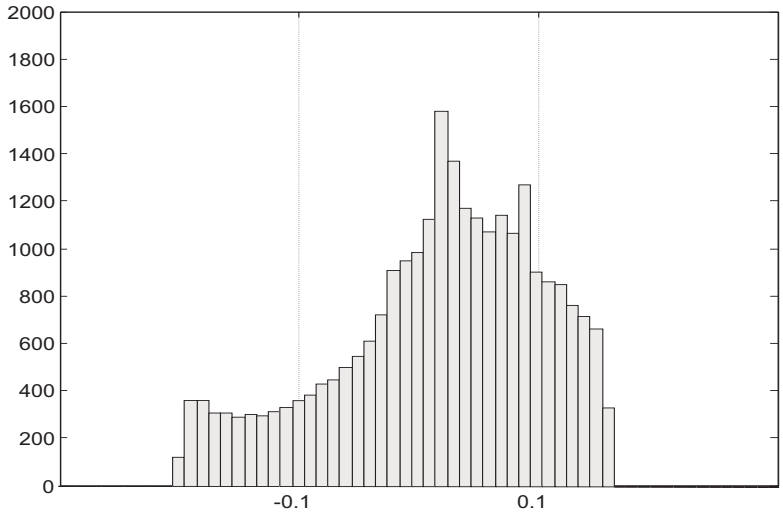

Figure 6: Histogram of differences between input and recovered vertical ionospheric delays

6 DETERMINATION OF DOUBLE DIFFERENCE CARRIER PHASE AMBIGUITIES

Real-time carrier-phase ambiguity determination has been studied extensively in the past. To study the additional value of using a sufficiently accurate ionospheric model, wide-lane $L_{WL} = (f1L1 - f2L2)/(f1 - f2)$, $L1$ and $L2$ ambiguities have been determined. For GEO satellite observations only L1 ambiguities could be determined. One major advantage of using wide-lane linear combinations (δ_{iono} = -0.283[cycles]) is that the remaining relative (in cycles) ionospheric error is significantly smaller Schaer (1999) compared to L1 (δ_{iono} = 1[cycles]) or $L2$ (δ_{iono} = 1.283[cycles]) respectively. Therefore wide lane ambiguities are less sensitive to ionospheric errors. Since the ionosphere de-correlates with an increasing baseline length only the impact on baselines longer than 50 km are considered in the paper. Using the $\nabla\Delta$ operators to denote the double-differences, the wide-lane observation can be written as:

$$\nabla\Delta L_{WL} = \nabla\Delta\rho + \nabla\Delta\delta_{trop} + \ldots$$
$$\nabla\Delta\delta_{ion,WL} + \lambda_{WL}\nabla\Delta N_{WL} + \nabla\Delta\varepsilon \qquad (9)$$

Looking at Equation 9 it is clear that to fix the integer ambiguities with a high level of reliability the remaining error components should not exceed 40 cm (WL/2). At the current stage the remaining multipath is neglected but since choke ring antennas have been used, it is not expected to exceed a few cm. To account for the tropospheric refractions the Saastamoinen model has been used. Both precise ephemeris and smoothed broadcast ephemeris have been used to reduce satellite orbit errors to the possible minimum of $\delta_{orbit} \sim$ 1m for the GPS satellites. The remaining orbit error for the GEO satellites outside any manoeuvres periods should not exceed 1m at the worst case. For both GPS and GEO satellites the resulting baseline error should not be more than a few millimetres considering baseline lengths of < 100km.

7 NUMERICAL RESULTS USING REAL DUAL-FREQUENCY DATA

The results were produced in a two-step process, firstly the determination of a *references* against which the performance of the processing strategy could be measured, and secondly, the application of the model and analysis. The data was captured in a test network containing 8 stations in the Greater London area. The baseline vectors vary between 1.2km and 92km. To verify the station coordinates the IGS station Herstmonceux (HERS) and the Ordnance Survey station London (LON) was included in the network. The station coordinates were determined using 2-hour dual-frequency data sets. The data was then processed with the Leica Ski-Pro software that was able to fix all the ambiguities. After a constrained adjustment sing the points LON and HERS as fixed points the uncertainty of the station coordinates did not exceed $\sigma_{pos,95\%}$ = 0.005m. Therefore the ”true” ambiguities could be determined to validate the ambiguities in the real-time experiment. At the present stage of the research only one baseline (52km) has been used. To test the new real-time processing strategy, the computations have been performed simulating a real-time scenario (i.e. computation of the baseline vector on a epoch-by-epoch basis). The following five scenarios where set to evaluate the benefit of including GEO-L1 observations and subsequently the derived ionospheric model:

- **Scenario 1:** Using all available GPS(9) and GEO(1) satellites above 15^o elevation.
- **Scenario 2:** Disabling 50% of all GPS satellite (all satellites towards North-East). Using the four remaining GPS satellites above 15 degree without any ionospheric correction. This is a simulation of a harsh positioning environment where the remaining visible satellites are in a degraded geometric configuration.
- **Scenario 3:** Disabling 50% of all GPS satellite (all satellites towards NE). Using the four remaining GPS satellites plus the GEO without any ionospheric correction.
- **Scenario 4:** Scenario 2 using the computed ionospheric model.
- **Scenario 5:** Scenario 3 using the computed ionospheric model.

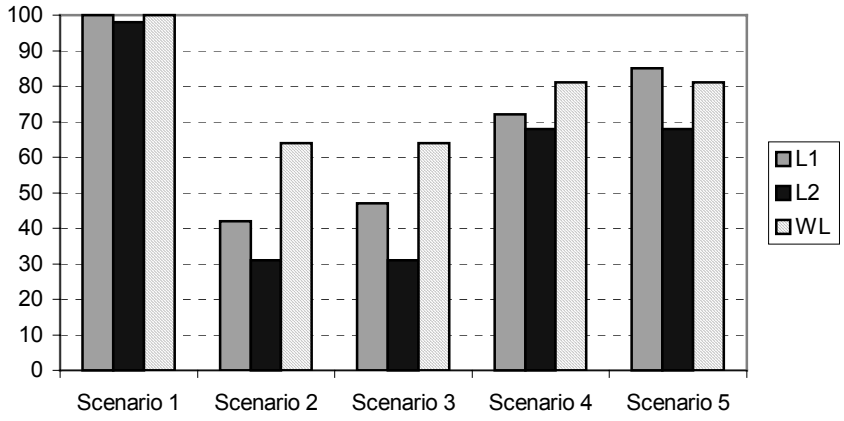

Figure 7 Performance for carrier-phase processing for different scenarios

Based on these examples the success rate for determining the carrier-phase ambiguities (i.e. rate of correctly determined ambiguities over one hour worth of data) has been increased considerable (Figure 7). Using the computed model has improved the success rate for the L1 ambiguities for PRN 120 (GEO) from 72% to 85% compared to the computation without any ionospheric model.

8 CONCLUSION

Ambiguity determination under harsh engineering conditions remains difficult. Although the approach presented here based on combining GPS and EGNOS GEO data and using a local ionospheric model leads to promising results, still ambiguities could not be determined all the time. However, for the scenarios investigated here where only two receivers are used, tomographic approaches for the determination of ionospheric delays are not adequate. Further research is required to investigate impact of the local model different baseline lengths. There is potential for optimising the weighting strategy within the ionospheric filtering, the spatial interpolation mechanism as well the integration of externally derived ionospheric models in the estimation process. Further research is required also to characterise the impact of different geometric conditions of the dual-frequency data points, on the accuracy of the local model.

9 REFERENCES

BROWN, R. G. AND HWANG, P. Y. C. (1983), *A Kalman filter approach to precision GPS geodesy*, Navigation: The Journal of The Institute of Navigation, 30(4):pages 338–349.

FELTENS, J. AND SCHAER, S (1998), *IGS products for the Ionosphere*, IGS Position Paper, IGS Analysis Centers Workshop ESOC, Darmstadt, Germany

Goad, C. C. (1990), *Optimal filtering of pseudoranges and phases from single-frequency GPS receiver*, Journal of Geodesy, 37(3):pages 249–262.

HANSEN, A., BLANCH, J., WALTER, T., AND ENGE, P. (2000), *Ionospheric correlation analysis for WAAS: Quiet and stormy*, in Proceedings of The 12th International Technical Meeting of the Satellite Division of the Institute of Navigation, Institute of Navigation, Salt Lake City, Utah.

HERNÁNDEZ-PAJARES, M., JUAN, J. M., SANZ, J., AND COLOMBO, O. L. (2000*), Application of ionospheric tomography to real-time GPS carrier-phase ambiguity resolution, at scales of 400-1000 km and with high geomagnetic activity*, Geophysical Research Letters, 27(13):pages 2002–2012.

LEICK, A. (1995), *GPS Satellite Surveying*, John Wiley & Sons Inc., New York.

LODDO, S; FLAMENT,D; BENEDICTO, J and MICHEL, P. (1996). *EGNOS, the European Regional Augmentation to GPS & GLONAS.* ION GPS-96: p1144

MOHAMED, A. H. AND SCHWARZ, K. P. (1999), Adaptive Kalman filtering for INS/GPS, Journal of Geodesy, 73:pages 193–203.

NovAtel Inc. (1997), *ProPak IITM OM-20000020* , Calgary, Canada, 2 edition.

SANDWELL, D. T. (1987), *Biharmonic spline interpolation of GEO-3and seasat altemeter data*, Geophysical resarch letters, 14(2):pages 139–147.

SCHAER, S. (1999), *Mapping and Predicting the Earths Ionosphere Using the Global Positioning System*, Ph.D. thesis, Universit¨at Bern.

SCHAER, S., BEUTLER, G., MEVART, L., ROTHACHER, M., AND WILD, U. (1995), *Global and regional ionosphere models using the GPS double difference phase observable frequency*, in Proceedings of the 1995 IGS Workshop, Silver Spring, MD, USA.

SUARD, N. (2000), *ESTB SIS user interface description*, Technical report, European Space Agency, GNSS-1 Project Office.